Hydrogen Production from Steam Reforming of Acetic Acid over Ni-Fe/Palygorskite Modified with Cerium

Yishuang Wang,[a,b] Mingqiang Chen,[a,b,*] Jie Yang,[b] Shaomin Liu,[a] Zhonglian Yang,[b] Jun Wang,[b] and Tian Liang [b]

The steam reforming of acetic acid (SRA) was carried out in a fixed-bed tubular reactor with Ni-Fe/ceria-palygorskite (CPG) catalysts. The as-prepared catalysts were analyzed by N_2 adsorption-desorption, scanning electron microscopy coupled with energy dispersive spectroscopy (SEM-EDS), H_2 temperature programmed reduction (H_2-TPR), and X-ray diffraction (XRD). The results of H_2-TPR and XRD showed that the addition of CeO_2 increased the hydrogen consumption of catalysts and the interaction force between active component (Ni-Fe alloy) and carrier. Moreover, the Ni-Fe alloys were successfully synthesized in the Ni-Fe/CPG catalysts and their crystallite sizes were decreased by adding CeO_2. In addition, these catalysts were employed to SRA at 600 °C, GHSV = 14427 h^{-1} and different molar ratio of S/C. The experimental results revealed that the Ni-Fe/$C_{0.4}PG_{0.6}$ catalyst can achieve the highest yield of H_2 (87%) and HOAc conversion (95%), as well as the highest stability during the process of steam SRA. Additionally, the spent catalysts were characterized by XRD, SEM, and thermogravimetric analysis (TGA). The results showed that the addition of CeO_2 enhanced the stability and activity of Ni-Fe/palygorskite catalyst and reduced the coke deposition rate on the catalyst surface.

Keywords: Steam reforming; Acetic acid; Hydrogen; Ni-Fe/CPG; Palygorskite; Carbon deposition

Contact information: a: School of Earth Science and Environmental Engineering and b: School of Chemical Engineering, Anhui University of Science and Technology, 232001, Huainan, PR China;
** Corresponding author: mqchen@aust.edu.cn*

INTRODUCTION

With declining fossil fuel reserves and growing ecological issues at present, clean and renewable energy sources are very favorably regarded. The utilization of hydrogen energy, which has the advantages of high calorific value and environmental friendliness, already meets the needs of clean energy. Hydrogen is also an important raw material used in ammonia synthesis and petroleum refineries (Kathe *et al.* 2016). However, most hydrogen is produced from fossil fuels (*e.g.*, coal, naphtha, and natural gas) or light hydrocarbons by reformer technology. This process always releases carbon dioxide into the atmosphere, causing the global warming problems and depleting fossil fuel reserves (Esteban-Díez *et al.* 2016). To reduce the consumption of these non-renewable resources, hydrogen production *via* pyrolysis, gasification, and steam reforming of biomass feedstock, which is carbon neutral and renewable, has been extensively studied (Rapagná *et al*. 2002; Bulushev and Ross 2011; Ma *et al.* 2014). Wu and co-workers investigated the effects of Ni content in catalysts and biomass components (cellulose, xylan, and lignin) on the hydrogen and syngas production *via* the steam pyrolysis-gasification technology in the two-stage fixed-bed. They found that hydrogen content was increased from 30.1 to 50.6 vol.% (the volume fraction in total gas composition) with the increase of Ni loading from

5 to 40 wt.% during the wood sawdust pyrolysis-gasification (Wu *et al.* 2011). They also revealed the compositions of biomass, gasification temperature, and the addition of steam had significant influence on hydrogen production (Wu *et al.* 2013). Additionally, the 2D dynamic model of biomass pyrolysis or steam reforming in two-stage fixed-bed reactors had been posed by Olaleye *et al.* (2014), and it agreed well with the experimental data in predicting the product and hydrogen yields from pyrolysis/steam reforming of different biomass feedstock at different reaction conditions. Although hydrogen production from these technologies is feasible and potential, the tar and particulates accompanying the product gas are always leading to blocking and fouling of process equipment, such as pipelines and turbines (Zhang *et al.* 2010). Furthermore, producing hydrogen from the above mentioned processes is of low economical value and relatively ineffective due to the high expenditure of collecting and delivering raw biomass feedstock and the low energy density of them (Chattanathan *et al.* 2012). Therefore, a promising scheme to generate hydrogen is to first carry out pyrolysis/gasification technology that converts biomass to bio-oil (Shen *et al.* 2015; Kan *et al.* 2016), which is subsequently reformed with steam for producing hydrogen. The viability of such a process is attributed to the fact that bio-oil is easier to transport and handle and has a higher energy density than biomass feedstock. It is well known that bio-oil is a complex mixture of alcohols, acids, ketones, esters, aldehydes, phenols, sugars, syringols, furans, guaiacols, and multifunction compounds (Trane *et al.* 2012). These oxygenated organic compounds endow bio-oil with many disadvantages, such as high viscosity, low hydrothermal stability, high corrosivity, and high oxygen content, all of which are important for large-scale utilization (Wang *et al.* 2013). Steam reforming (SR) can be applied to convert the real bio-oil or each of the bio-oil components to H_2-rich gas. Thermodynamic calculations and experimental results of reforming of model compounds of bio-oil, ethanol (Iulianelli *et al.* 2016), acetic acid (HOAc), acetone (Li *et al.* 2012), ethylene glycol (Mei *et al*. 2016), and phenol (Koike *et al.* 2015) show that the components in the presence of steam can be easily converted to H_2-rich gas, reaching the maximum H_2 yield (65 to 90%) at different temperatures under ambient pressure and a steam/carbon (S/C) ratio greater than 1.

Hydrogen production has been examined during the steam reforming of acetic acid (SRA), which is a major component in bio-derived compounds and constitutes 12 to 30% of bio-oil (Basagiannis and Verykios 2007; Vagia and Lemonidou 2007; Basagiannis and Verykios 2008; Hu and Lu 2010; Li *et al.* 2012; Mohanty *et al.* 2012; Pant *et al.* 2013; Wang *et al.* 2015; Esteban-Díez *et al.* 2016; Wang *et al.* 2016). The effect of transition metals (*e.g.*, Ni, Co, Fe, Cu, and Zn) and noble metals (*e.g.*, Pd, Pt, Rh, and Ru) and the individual/mixture of the support (*e.g.*, Al_2O_3,CeO_2, La_2O_3, and MgO) on SRA has been abundantly studied. Noble metals, especially Ru, loaded on different carriers have more significant activity than transition metals for SRA. Basagiannis and Verykios (2007) demonstrated that Ru-based and Ni-based catalysts loaded on different metal oxides carriers, such as Al_2O_3, MgO/Al_2O_3, CeO_2/Al_2O_3, and La_2O_3/Al_2O_3, showed high activity and selectivity to H_2. They also revealed that the stability of Ru-based catalysts was higher than that of Ni-based catalysts in long-term SR. Bossola *et al*. (2016) conducted the experiment of SRA over Mg(Al)O supported Ru-based and Rh-based catalysts, which had very low loading of active metal (0.5 wt.%), at 700 °C and S/C = 3. The Ru catalysts reached 100% conversion of HOAc and hydrogen yield higher than 70%. Although noble metal catalysts are highly efficient for SRA, their expensive price makes them not suitable for industrial manufacture. Therefore, lower-cost transition metal catalysts have been investigated (Basagiannis and Verykios 2006; Hu and Lu 2010; Wang *et al.* 2012; Zhang

et al. 2014; Wang *et al* 2015, 2016; Pandey and Deo 2016). Among the transition metals, Ni-based catalysts have high-activity in SRA for H_2 production. Hu and Lu (2010) investigated the reaction of SRA for hydrogen production over transition metals, such as Ni, Co, Fe, and Cu supported on Al_2O_3. The Ni/Al_2O_3 and Co/Al_2O_3 catalysts had a significant activity among these catalysts, which was attributed to their high activity for cracking C-C and C-H bonds, but the performance of Ni/Al_2O_3 catalyst was much more stable than that of Co/Al_2O_3 in a long-term reaction. However, monometallic nickel can be sintered easily at high temperature and suffers low anti-carbon deposition performance, resulting in Ni-based catalysts easily becoming deactivated (An *et al.* 2011). To solve these problems, bimetallic catalysts, such as Ni-Fe (Koike *et al*. 2015; Wang *et al.* 2015), Ni-Co (Pant *et al.* 2013; Yue *et al*. 2015), and Ni-Cu (Lytkina *et al*. 2015), have been applied in catalytic reforming for H_2 production and many catalyst carriers with high oxygen storage capacity (*e.g.*, CeO_2 and La_2O_3) (Remiro *et al.* 2013; Zhang *et al.* 2014; Osorio-Vargas *et al.* 2016) have been introduced into Ni-based catalysts.

For the sake of economic efficiency, there are also many low-cost mineral material carriers; perovskite (Ramesh *et al*. 2015), olivine (Świerczyński *et al.* 2007), and palygorskite (attapulgite) (Wang *et al.* 2015, 2016) that have been used in nickel-based catalysts for steam-reforming oxygenated hydrocarbons. Among them, Palygorskite (PG), also called attapulgite, has obtained more and more attention in recent studies, which is mainly because it is a natural nonmetallic mineral with a 1-D fibrous morphology and has a unique porous crystalline structure containing tetrahedral and octahedral layers. In addition, due to its special structure, low cost, and easy availability, PG clay is widely applied in chemicals, surface coating, and catalysis (Li *et al.* 2013; Laosiripojana *et al.* 2014; Guo *et al.* 2015). Cao *et al.* (2008) studied low-temperature CO oxidation over a series of CuO supported on PG catalysts, which showed interesting catalytic activity compared with the reported TiO_2, Fe_2O_3, and $Ce_{0.8}Zr_{0.2}O_2$ supported CuO catalysts. Notwithstanding PG (as a catalytic carrier) has these unique structure and physicochemical properties, it is rarely applied to SRA. In order to extend the application of PG and optimize the product distribution of SRA, in our recent research (Wang *et al.* 2016), PG was selected as a catalyst support to prepare different Ni/ATP (attapulgite) catalysts for SRA, which exhibited an outstanding HOAc conversion efficiency (95%) and H_2 yield (82%). Unfortunately, there was some amount of coke deposited on the catalyst surface, and their stabilities were decreased after 4 h of reaction time. This can be attributed to two major drawbacks of metallic nickel supported on attapulgite; such combinations have a high tendency to sinter and to form carbonaceous species, leading to severe deactivation. These undesirable attributes can be minimized by adding other metals/ metallic oxide as promoters to the catalytic system. Among these promoters, as has been reported by Laosiripojana *et al.* (2014), metallic iron and CeO_2 are available and efficient for Ni-based catalysts. Iron species, as one of the ingredient of active phase, not only can change the redox properties of Ni-based catalysts by forming Fe_2O_3 or Fe_3O_4, but also produce the Ni-Fe alloy upon the interaction between Ni and Fe (Abelló *et al.* 2013; Bolshak *et al.* 2013). Additionally, CeO_2 also has promising redox properties and high oxygen vacancy and mobility, which can promote the gasification of carbonaceous species deposited on the catalyst (Perrichon *et al.* 1994; Zhang *et al.* 2014; Li *et al.* 2015). Therefore, the specialties of iron and ceria could restrain the sintering of active metallic nickel and the forming of coke precursor, and then enhance the activity and stability of Ni-based catalyst.

However, these effective and promising facilitators have not been studied in the Ni/PG system. According to our previous study (Wang *et al.* 2015), it was shown that the

Ni-Fe/PG catalyst with the Ni:Fe molar ratio of 1:1 exhibited outstanding activity and H_2 selectivity. In this paper, we focus on the addition of CeO_2 and the effect of Ni-Fe/PG catalyst on the catalytic performance and gaseous product distribution. Firstly, we modified the raw PG with CeO_2 by using mechanical blending method to produce carriers, and then they were recorded as C_xPG_{1-x}. Subsequently the Ni-Fe bimetallic catalysts loaded on C_xPG_{1-x} were prepared using a co-precipitation method. Furthermore, the prepared catalysts were applied into SRA at 600 °C, GHSV = 14427 h^{-1}, and different S/C (1~9). The yield of H_2, the conversion of HOAc and the distribution of gaseous products in the process of SRA over these catalysts were detected. In addition, the effect of CeO_2 on the reactive activity, the stability, and the anti-carbon deposition ability were also investigated.

EXPERIMENTAL

Raw Materials

All precursors and chemicals used for catalyst preparation were of high purity (99.9%) and purchased from Sinopharm Chemical Reagent Co., Ltd. (Shanghai, China). $Ni(NO_3)_2 \cdot 6H_2O$ and $Fe(NO_3)_3 \cdot xH_2O$ were used for preparing the catalysts precursors of nickel and iron. CeO_2 was commercial and Palygorskite was collected from SuZhou of Anhui Province.

Catalysts Preparation

Mechanical blending method for CeO_2/ Palygorskite (CPG) supports

First, 10 g of PG and *n* g CeO_2 (*n* = 1.11, 2.22, 4.29, and 6.67, respectively) were dispersed into absolute ethyl alcohol to form turbid liquid. The mixture was placed in an agate jar assembled in an ND7-1L ball grinder and ground for 4 h at a revolving speed of 200 r/min. Filter cakes were collected from the suspension by suction filtration, oven-dried at 105 °C for 12 h, ground into powders, and finally calcined at 550 °C with the heating rate of 2 °C/min for 2 h. A series of CPG carriers were prepared though these procedures, which were represented as C_xPG_{1-x} (x = 0.1, 0.2, 0.3, 0.4; representing weight percent).

Co-precipitation method for Ni-Fe/ CeO_2/ Palygorskite (NF/ CPG) catalysts

In previous work (Wang *et al.* 2015), a Ni-Fe bimetallic catalyst, with a molar ratio of Ni:Fe = 1:1, showed outstanding activity for steam reforming of bio-oil and achieved superior yield of H_2. Therefore, the nickel and iron species (1:1 of Ni:Fe molar ratio) were loaded on the series of CPG carriers *via* co-precipitation. $Ni(NO_3)_2 \cdot 6H_2O$ and $Fe(NO_3)_3 \cdot xH_2O$ as nickel and iron precursors were thoroughly mixed 100 mL of deionized water in a round-bottom flask and then placed in thermostat water bath with magnetic stirring at 80 °C for 2 h. A certain amount (10 g) of CPG was added into the system before being fully stirred at 80 °C for 2 h. Next, 2.5 M ammonia hydroxide was added dropwise into this solution until the pH reached 7.5 ± 0.5 and the precipitate was obtained. The precipitate was filtered, washed with deionized water, dried at 105 °C for 12 h, calcined at 550 °C with the heating rate of 2 °C/min for 2 h, pelletized, and crushed into 80 mesh with a sifter. The prepared fresh catalysts were denoted NF/C_xPG_{1-x} (x = 0.1, 0.2, 0.3, 0.4).

Catalyst Characterization

The crystal phases of catalysts were identified with a DanDong HaoYuan DX-2800 X-ray Diffractometer (Dandong, China), using Cu-Kα radiation (λ = 1.5406 Å, 40 kV, 30

mA) in the 2θ range of 5 to 70° at a scanning step of 0.03°. The morphologies were observed by Hitachi S-4800 Scanning Electron Microscope (SEM; Hitachi, Japan) coupled with Energy Dispersive Spectroscopy (EDS). The element compositions of all as-prepared catalysts were detected with Inductively Coupled Plasma Optical Emission Spectrum (ICP-OES, Varian, USA). The textual properties of all fresh catalysts were measured by the N_2 adsorption-desorption isotherms at liquid nitrogen temperature (77 K), using an ASAP2020 surface area and porosity analyzer (Norcross, USA). The surface area of catalyst was calculated by the Brunauer-Emmett-Teller (BET) method, the cumulative volume of catalyst pores was calculated from BJH desorption isotherm, and the average pore diameter was calculated from BJH desorption isotherm. Temperature Programmed Reduction (H_2-TPR) was performed using a TianJin PengXaing PX200 chemical adsorption instrument (Tianjin, China), in which the H_2 consumption was determined with a Thermal Conductivity Detector (TCD). A total of 100 mg of catalyst was added into the bed-reactor and reduced with a 5% H_2/Ar (v/v) mixture flowing at 40 mL·min^{-1} for each measurement. In this process, the reaction temperature was raised from room temperature to 900 °C at a heating rate of 10 °C·min^{-1}. Thermogravimetric analysis (TGA) of spent catalysts was performed on the TGA/DSC1 STAR^e System instrument (Mettler-Toledo, Switzerland) under air (50 mL/min) heating from room temperature to 900 °C at a heating rate of 10 °C/min to detect the amount and types of coke deposit.

Experimental Setup and Methods

The SRA was carried out in a fixed-bed tubular reactor under atmospheric pressure at 600 °C. This reactor was made of high-temperature resistance stainless steel, with an inner diameter of 30 mm and an overall length of 300 mm. A porous distributor was placed 200 mm away from the top of the reactor to support the catalytic material. The reaction temperature was monitored and controlled by two thermocouples: one was inserted into the center of the reactor while the other was placed between the furnace and the tube. The flow rates of carrier gas (99.99% N_2) and reducing gas (10% H_2/N_2, v/v) were measured by two glass rotameters. The raw material was introduced into the system by a constant flow pump. The schematic layout of the experimental device is shown in Fig. 1.

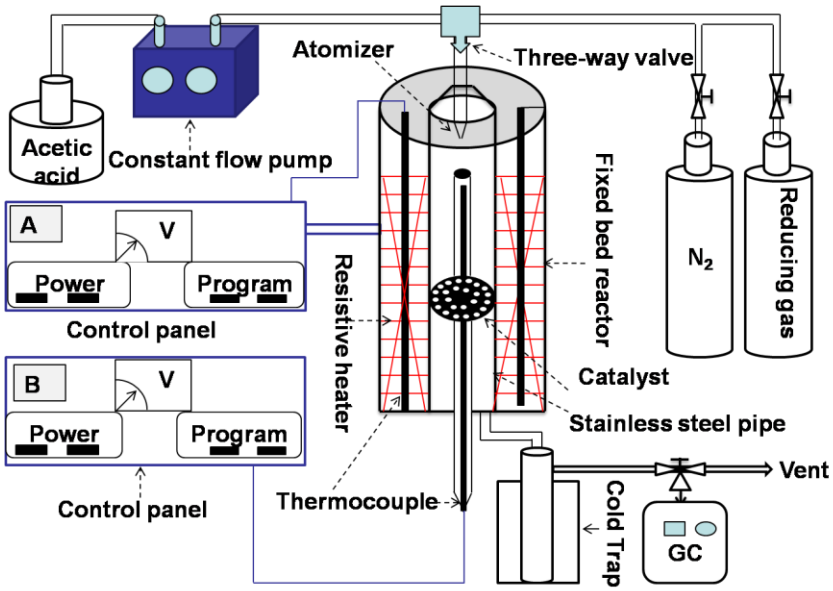

Fig. 1. Schematic diagram of experimental device

Prior to every experiment, some amount of catalyst was placed on the porous distributor and activated under the H_2/N_2 (*v*/*v* = 10%, flow velocity, 0.32 $L \cdot min^{-1}$) atmosphere at 600 °C for 2 h. The gaseous products were collected by airbags and analyzed with gas chromatography (Shanghai Huaai, GC9160) equipped with 5 Å molecular sieve (measures H_2, CH_4, and CO) and Porapak Q column (measures CO_2) by using Thermal Conductivity Detector (TCD) The condensed liquid phases were analyzed by Agilent 6820 60m DB-Wax capillary column. The liquid products were mainly acetone and un-reacted HOAc.

The overall process of SRA is complex, which includes a set of elementary steps involving several organic intermediates and various secondary reactions, according to different catalysts and operating conditions. The thermal decomposition mechanisms of HOAc can be dated back to the year of 1969 and were reported by Blake and Jackson (1969). After that Wang *et al.* (1996) and Marquevich *et al.* (1999) studied the involved reactions during the process of SRA. Meanwhile, according to the resent studies (Mohanty *et al.* 2012; Nogueira *et al.* 2014; Wang *et al.* 2015), the favorable reactions can be summarized by R1-R7.

$$CH_3COOH \xrightarrow{H_2O} 2CO + 2H_2 \quad \Delta H^0_{298K} = 213.4\ kJ/mol \tag{R1}$$

Water gas shift reaction (WGSR):

$$CO + H_2O \xleftrightarrow{catalyst} CO_2 + H_2 \quad \Delta H^0_{298K} = -41\ kJ/mol \tag{R2}$$

The overall reaction of steam reforming may be represented as following:

$$CH_3COOH + 2H_2O \xrightarrow{catalyst} 2\ CO_2 + 4H_2 \quad \Delta H^0_{298K} = 131.4\ kJ/mol \tag{R3}$$

$$CH_3COOH \rightarrow \text{Gases } (H_2, CH_4, CO, CO_2 \ldots) + \text{Coke} \tag{R4}$$

$$2CH_3COOH \rightarrow CH_3COCH_3 + CO_2 + H_2O,\ \Delta H^0_{298K} = 16.7\ kJ/mol \tag{R5}$$

$$CO + 3H_2 \rightarrow CH_4 + H_2O,\ \Delta H^0_{298K} = -206.1\ kJ/mol \tag{R6}$$

$$CO_2 + 4H_2 \rightarrow CH_4 + 2H_2O,\ \Delta H^0_{298K} = -165.1\ kJ/mol \tag{R7}$$

In the process of SRA for hydrogen generation, the theoretical maximum yield of H_2 is 4 mole per mole of acetic acid. On the basis of elemental balance, the conversion of HOAc and the yield of H_2 could be calculated with equations, and the related assumptions on fuel have been reported by Pimenidou *et al.* (2010).

The molar flow rate of total dry outlet gas ($n_{out,dry}$) can be calculated based on nitrogen balance (Eq. 1). In which y is represent the molar flow of i species (such as H_2, CH_4, CO, CO_2, C_2, and C_3) in outlet gas.

$$n_{out,dry} = \frac{n_{N_2}}{1 - y_{CH_4} - y_{CO} - y_{CO_2} - y_{H_2} - y_{C_2} - y_{C_3}} \tag{1}$$

The conversion of HOAc (X_{HOAc}) can be estimated based on carbon balance, with the total molar flow of carbon in the gaseous products being divided by the molar flow of carbon in feed, as described in Eq. 2.

$$X_{HOAc}\ (\%) = \frac{n_{out,dry} \times (y_{CO} + y_{CH_4} + y_{CO_2} + 2y_{C_2} + 3y_{C_3})}{2n_{HOAc,in}} \times 100 \tag{2}$$

The yield of H_2 (Y_{H2}) is defined as the percentage of experimental H_2 yield in theoretical maximum H_2 yield according to (R3) (Eq. 3).

$$Y_{H_2}(\%) = \frac{n_{out,dry} \times y_{H_2}}{4n_{HOAc,in}} \times 100 \quad (3)$$

In order to remove the effect of N_2 and compare the gas concentration of component, the distribution (f_i, %) of gas product can be obtained by Eq. 4.

$$f_i(\%) = n_i/\left(n_{H_2} + n_{CH_4} + n_{CO} + n_{CO_2}\right) \times 100 \quad (4)$$

RESULTS AND DISCUSSION

Catalyst Characterizations

The textural properties and chemical compositions of all samples

The textural properties (*e.g.* the surface area, cumulative volume of pores, and the average pore diameter) of fresh catalysts were measured by N_2 adsorption-desorption, and the calculated values are presented in Table 1. Additionally, the N_2 adsorption-desorption isotherms and pore size distributions of PG, NF/PG and NF/$C_{0.4}PG_{0.6}$ were displayed in Fig. 2. From these information, it can be seen that the series of NF/C_xPG_{1-x} showed advantageous surface area (125 to 175 $m^2 \cdot g^{-1}$) and regular pore diameter (7 to 10 nm).

Table 1. The Textural Properties of All Fresh Samples

Samples	S_{BET} [a] ($m^2 \cdot g^{-1}$)	V [b] ($cm^3 \cdot g^{-1}$)	d_{pore} [c] (nm)	Average Particle Size/(nm)
PG	145	0.444	15.0	41
NF/PG	175	0.453	9.8	34
NF/$C_{0.1}PG_{0.9}$	147	0.389	10.1	40
NF/$C_{0.2}PG_{0.8}$	135	0.296	8.1	44
NF/$C_{0.3}PG_{0.7}$	136	0.282	7.8	45
NF/$C_{0.4}PG_{0.6}$	125	0.228	7.1	48

[a] Surface area (S_{BET}) calculated by Brunauer-Emmett-Teller (BET) method; [b] V is cumulative volume of pores calculated from BJH desorption isotherm. [c] d_{pore} is average pore diameter calculated from BJH desorption isotherm.

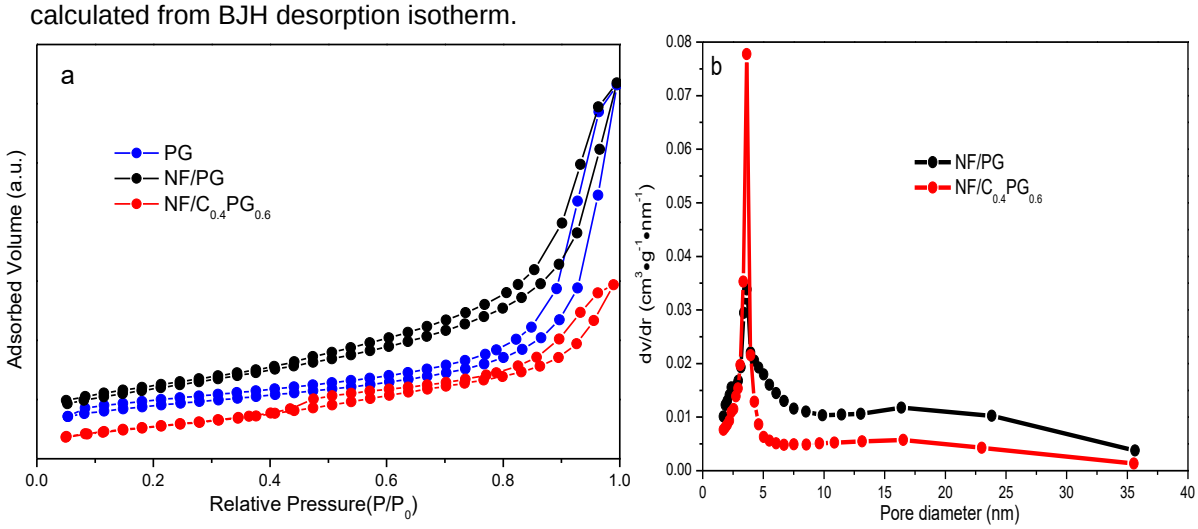

Fig. 2. (a) N_2 adsorption-desorption isotherms of PG, NF/PG and NF/$C_{0.4}PG_{0.6}$ samples; (b) pore size distribution of NF/PG and NF/$C_{0.4}PG_{0.6}$ catalysts

The chemical content of catalyst carriers were shown in Table 2, from which it could be seen that PG was be made up of SiO_2, Al_2O_3, MgO, and Fe_2O_3. Notably, the CeO_2 content in $C_{0.1}PG_{0.9}$, $C_{0.2}PG_{0.8}$, $C_{0.3}PG_{0.7}$, and $C_{0.4}PG_{0.6}$ samples was 11.3%, 18.8%, 27.1%, and 38.8%, respectively, they were almost equal to the nominal content of CeO_2.

Table 2. Chemical Composition of Catalyst Supports (wt.%)

Samples	SiO_2	Al_2O_3	MgO	K_2O	TiO_2	Fe_2O_3	CeO_2
PG	76.1	8.7	7.7	1.3	0.9	5.3	/
$C_{0.1}PG_{0.9}$	65.8	8.5	7.8	0.8	0.7	5.1	11.3
$C_{0.2}PG_{0.8}$	60.3	7.6	7.5	0.7	0.9	4.2	18.8
$C_{0.3}PG_{0.7}$	52.9	7.3	7.1	0.6	1.1	3.9	27.1
$C_{0.4}PG_{0.6}$	42.5	8.0	6.2	0.6	0.4	3.5	38.8

In addition, the chemical compositions of all catalysts are presented in Table 3. The contents of NiO and Fe_2O_3 in Ni-Fe bimetallic catalysts were roughly equal to each other. It is worth noting that the content of Fe_2O_3 was higher than that of NiO in one catalyst. In other words, the practical content of Ni:Fe molar ratio was lower than that of nominal mole ratio (Ni:Fe = 1:1). This was caused by the small amount of additional Fe_2O_3 content in PG (Table 1), although the mole proportion of Ni to Fe added into catalyst was 1 during the process of catalyst preparation. In order to further investigate the actual content of Ni and Fe in every catalyst, the catalysts were analyzed by ICP-OES and the result was shown in Table 4. It also testified the actual content of Ni:Fe was little lower than that of nominal mole ratio 1.

Table 3. Chemical Composition of All Fresh Catalysts (wt.%)

Samples	SiO_2	Al_2O_3	MgO	K_2O	TiO_2	NiO	Fe_2O_3	CeO_2
NF/PG	60.2	8.2	7.4	1.0	0.6	9.4	13.2	/
NF/$C_{0.1}PG_{0.9}$	51.2	6.8	6.8	0.7	0.6	10.2	14.6	9.1
NF/$C_{0.2}PG_{0.8}$	48.0	6.4	6.5	0.5	0.6	9.5	13.2	15.3
NF/$C_{0.3}PG_{0.7}$	41.6	5.6	6.4	0.7	1.1	9.2	13.3	22.1
NF/$C_{0.4}PG_{0.6}$	32.7	6.9	7.2	0.7	0.7	9.1	12.6	30.1

Table 4. Element Composition of Calcined Catalysts Obtained by ICP-OES

Samples	Si	Al	Mg	Ni	Fe	Ce
PG	3.7	5.1	5.6	/	3.9	/
NF/PG	6.8	3.3	3.6	6.5	8.8	/
NF/$C_{0.1}PG_{0.9}$	0.8	0.6	0.3	7.1	7.6	1.3
NF/$C_{0.2}PG_{0.8}$	0.8	2.4	1.9	7.5	9.1	3.4
NF/$C_{0.3}PG_{0.7}$	0.6	0.3	0.3	6.3	7.8	4.6
NF/$C_{0.4}PG_{0.6}$	2.2	4.7	3.9	6.6	10.0	5.2

Scanning electron microscopy (SEM)

The SEM micrographs of raw PG and fresh prepared NF/$C_{0.4}PG_{0.6}$ are shown in Figs. 3a and 3b. Raw PG was fibrous or clubbed structure in its surface, every fiber or rod was smooth, and there were some small ravines present among different ribbons and interlaminations. Thus, the unique structure of PG could supply a high specific surface area (145 $m^2 \cdot g^{-1}$, as shown in Table 1) (Guo *et al.* 2015). Figure 3b shows that the surface of NF/$C_{0.4}PG_{0.6}$ sample was relatively rougher than the raw PG. There were many spherical rough particles adhered on the surface of PG, and they were attributed to nickel-iron and

CeO_2 particles were located among different ribbons and interlaminations. In addition, the form of spherical rough particles was ascribed to the synthetic interaction among nickel-iron oxide, cerium dioxide, and PG particles. This situation could cause the catalyst specific area to decrease from 145 $m^2 \cdot g^{-1}$ to 125 $m^2 \cdot g^{-1}$ and pore volume to reduce from 0.444 $cm^3 \cdot g^{-1}$ to 0.228 $cm^3 \cdot g^{-1}$, as shown in Table 1.

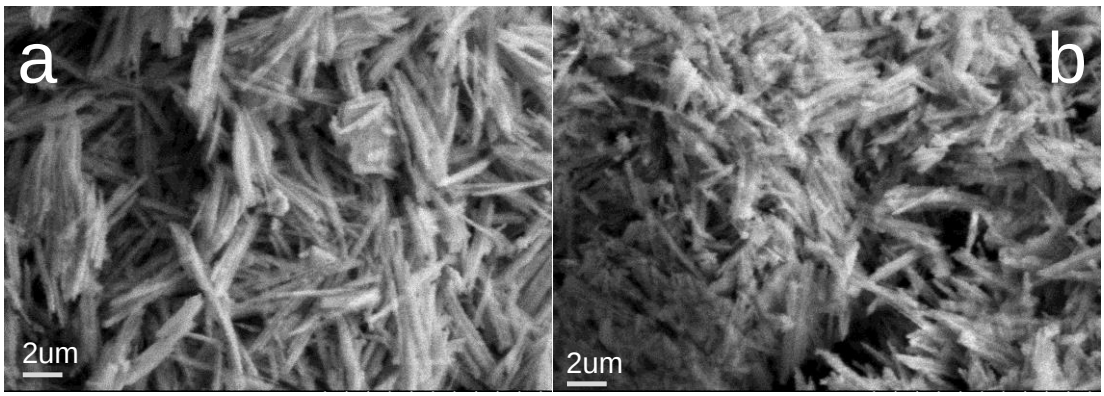

Fig. 3. SEM images of catalysts: (a) raw PG; (b) NF/$C_{0.4}PG_{0.6}$

Temperature programmed reduction (H_2-TPR)

The reducibility of supports and catalysts was analyzed with H_2-TPR, and the results were presented in Fig. 4. There are two reduction peaks related to CeO_2, which have been described in the literature (Yao *et al.* 1984; Perrichon *et al.* 1994). The one located at 570 °C (peak β) was attributed to the reduction of the CeO_2 surface oxygen; the other peak at 890 °C (peak η) was associated with the reduction of bulk part of CeO_2, which emerged through removing the reactive oxygen species (O^{2-}) from the reticulum and forming the Ce_2O_3 ($2CeO_2 + H_2 \rightarrow Ce_2O_3 + H_2O$). Obviously, there was no significant peak of PG support, as shown in Fig. 4a, which demonstrated that PG could not be easily reduced. It also can be seen from Fig. 4a, the center temperature of the two peaks β and η, which belong to the reduction peaks of CeO_2, was removed to a lower temperature than those described in the literature. Furthermore, the intensities of peaks β and η of C_xPG_{1-x} supports (Fig. 4a) tended to increase with increasing CeO_2, which indicated that the addition of CeO_2 increased the hydrogen consumption and surface oxygen of catalyst carriers. This point will be further certified by TG-DSC analysis for spent catalyst in a later section.

Additionally, there were two apparent peaks (α and γ) that emerged in calcined catalysts (Fig. 4b). In the sample of NF/PG, the peak α was a broad overlapping peak within the temperature range of 350 °C to 700 °C, which represented the reduction of Ni-Fe oxides that had weak interaction with carriers to form Ni-Fe alloy. This result was also demonstrated by XRD of reduced catalysts (Fig. 5b). After the insertion of CeO_2, the center temperature of reduction peak α was slightly increased, and the temperature range was slightly constricted with the increased CeO_2. This phenomenon was ascribed to addition of CeO_2 into NF/PG catalyst enhanced the interaction of nickel-iron alloys and improved the coactions among different catalyst components of the series of NF/CPG catalysts. The other peak γ located at 650 °C was attributed to the reduction of Ni-Fe oxides that had strong interaction with carriers to produce Ni-Fe alloy. In addition, the center temperature of peak γ was increased with the addition of CeO_2. This finding further demonstrated that CeO_2 could promote the interaction between active metal and carrier and increase the

catalyst stability, which had been demonstrated in the stability test section. Obviously, the characteristic peaks of PG at 2θ = 50.06° and 59.83° gradually disappeared with the increase of CeO_2, and the intensities of characteristic peaks at 2θ = 20.33° and 26.66° were weakened. This result revealed that the crystallization of PG changed slightly after inserting CeO_2 into its structural framework.

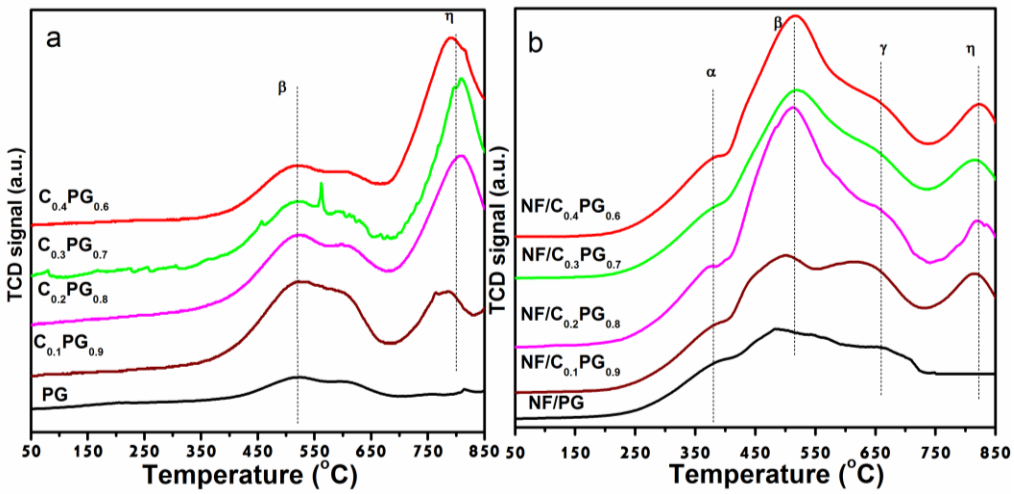

Fig. 4. H_2-TPR profiles: (a) the catalyst carriers and (b) the calcined catalysts

X-ray diffraction analysis

Figure 5 shows the XRD patterns of all fresh catalysts and reduced catalysts after the H_2 reduction at 600 °C for 2 h. As shown in Fig. 5a, the peaks at 2θ = 20.33° and 26.66° were the typical characteristic peaks of PG (JCPDS 31-0783), and the peaks 50.06° and 59.83° were attributed to dolomite (JCPDS 99-0046) (Wang *et al.* 2016). Their intensities were decreased and even disappeared with the addition of CeO_2. This may have been due to the interaction between PG and CeO_2 (You *et al.* 2010). The diffraction peaks at 2θ = 28.55°, 33.08°, 47.51°, 56.36°, 59.01°, and 69.44° were well defined and belonged to CeO_2 (JCPDS 81-0792) with a fluorite structure presented in the catalysts.

In NF/PG, the characteristic diffraction peaks of PG were not changed, and the characteristic diffraction peaks of nickel oxide and iron oxide or their synthesis could not be detected, as shown in Fig. 4a. When the catalysts were reduced with H_2 at 600 °C for 2 h, the characteristic diffraction peaks of PG and CeO_2 were not significantly changed (Fig. 4b), which was mainly because CPG supports were hard to reduce at 600 °C. This result was confirmed by H_2-TPR (Fig. 3). This further demonstrated the interaction between CeO_2 and PG. However, when Ni and Fe species were introduced, a broad and low-intensity diffraction peak at 2θ = 44.01° was observed, as shown in Fig. 4b. In previous studies, Laosiripojana *et al.* (2014) and Pandey and Deo (2016) developed the Ni-Fe bimetallic based catalysts supported by different carriers for reforming biomass tar and catalyzing CO_2 methanation reaction. During analyzing the as-prepared catalysts by XRD, they also found the diffraction peaks at ~44° in reduced catalysts and established that they belong to the characteristic peak of Ni-Fe (111) alloy. Therefore, the peaks at 44.01° in reduced NF/PG and NF/C_xPG_{1-x} were attributed to the Ni-Fe alloys with crystal face (111). These results indicated that the absence of nickel and iron diffraction peaks before reduction (Fig. 5a) could be due to the high dispersion of nickel oxide and iron oxide

particles on the surface of CPG supports or to the formation of nickel and iron amorphous crystallization, which could not be detected with XRD. In addition, as shown in Table 5, the Ni-Fe alloy particle size, which was calculated by the Scherrer equation based on the (111) lattice plane parameters in XRD analysis, decreased from 15.5 nm (NF/PG,) to 8.9 nm (NF/$C_{0.4}PG_{0.6}$,) with the addition of CeO_2. The variation further revealed that CeO_2 addition enhanced the dispersion of catalyst active phases (Ni-Fe alloy) on the carrier. Previous studies uncovered that Ni-Fe alloys are successfully synthesized on the surface of catalyst support using nickel and iron as raw materials because nickel and iron atoms have a similar electronic orbit structure and metallic magnetism (Świerczyński *et al.* 2007; Wang *et al.* 2011; Pandey and Deo 2016). Therefore, the emerged broad diffraction peaks at 2θ = 44.01° in these synthetic catalysts were due to the formation of Ni-Fe alloy phases.

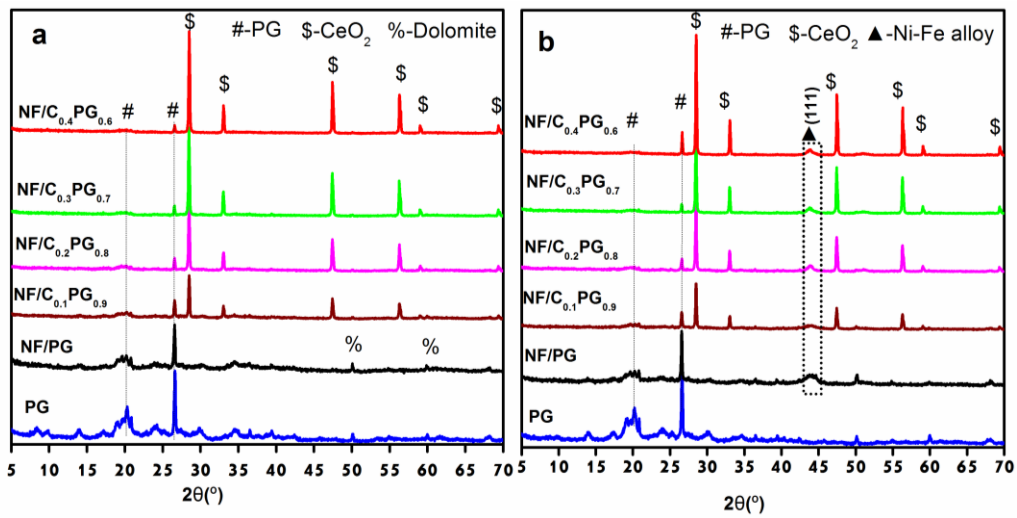

Fig. 5. XRD patterns of catalysts: (a) calcined catalysts; (b) reduced catalysts

Table 5. The Calculated Values of Ni-Fe Alloy Size at 2θ = 44.01° in Reduced and Spent Catalysts by Scherrer Equation from XRD Data

Samples	The crystallite size (nm) of formed Ni-Fe alloy (111)	
	Reduced catalysts	Spent catalysts
NF/PG	15.4	26.3
NF/$C_{0.1}PG_{0.9}$	12.8	15.5
NF/$C_{0.2}PG_{0.8}$	13.5	14.6
NF/$C_{0.3}PG_{0.7}$	11.8	13.7
NF/$C_{0.4}PG_{0.6}$	8.9	10.0

Catalytic Activity Tests

Activities of all catalysts

The operation of SRA was performed under the following conditions: temperature at 600 °C, S/C = 3, GHSV = 14427 h^{-1} , and time on steam for 4 h. Figures 6a and 6b show the time-dependent variations of X_{HOAc} and Y_{H2} for all catalysts during SRA, and Fig. 6c shows the distribution of gaseous products (H_2, CO, CO_2, and CH_4). The X_{HOAc} and Y_{H2} resulting from the reaction in the presence of NF/PG catalyst were approximately 80% and 52%, respectively, which were remarkably higher than those in the blank test using PG as a catalyst (approximately 50% and 5%, respectively). The concentrations of CH_4 and CO_2 (Fig. 6c) reached the highest levels, while the concentration of H_2 was at its lowest value

in the PG sample. Figure 6c also shows that the concentrations of H_2 and CO increased to 45% and 32% over the NF/PG catalyst. This was because PG had no obvious activity for SRA, and the temperature was the only major active factor in the situation, in which the thermal decomposition of HOAc (R4) and ketonization (R5) became predominant under this temperature, as these reactions were endothermic.

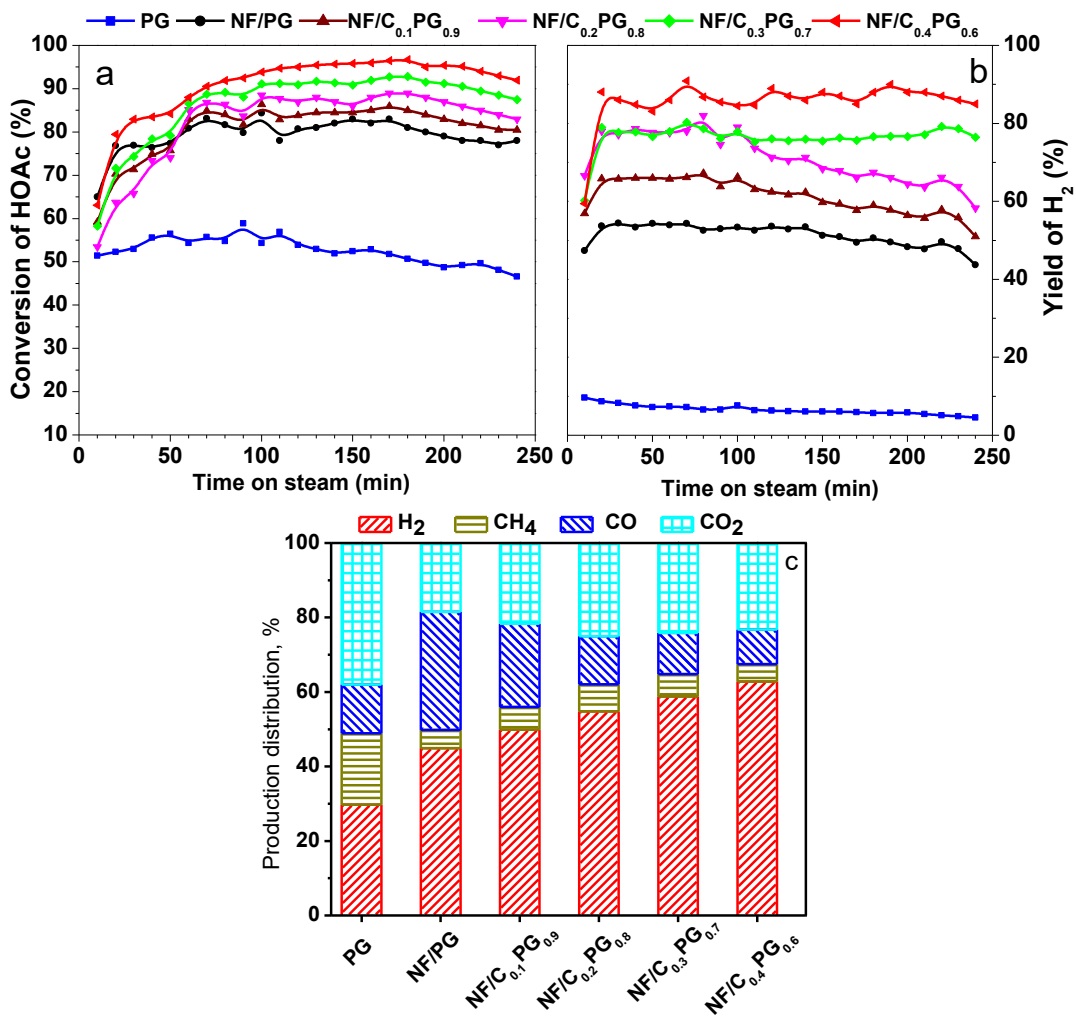

Fig. 6. Effect of different catalysts on (a) the conversion of HOAc and (b) the H_2 yield with time on steam; (c) the production distribution over all catalysts during the process of SRA

In addition, the X_{HOAc} and Y_{H2} increased markedly as nickel-iron species were introduced into PG accompanied with the increases of H_2 and CO concentrations. This result reflected that nickel and iron species accelerated the decomposition of HOAc and facilitated the steam-reforming reaction of HOAc and intermediate species, such as acetone and CH_4 **(**R3, R8-R10) (Laosiripojana *et al.* 2014); Ni has a strong ability for breaking C-C bonds, and Fe could promote a steam-reforming reaction of intermediates. When different amounts of CeO_2 were added into the NF/PG catalyst, the X_{HOAc} increased from 80% to 95%, accompanied by an increase in H_2 yield from 52% to 87% (Figs. 6a, b). The concentrations of CH_4 and CO noticeably decreased (Fig. 6c). This phenomenon was attributed to the superior properties of CeO_2 in terms of its high oxygen storage capacity and the high oxygen mobility (as proven by H_2-TPR), which improved carbon gasification

(R12) on the catalyst surface (Zhang *et al.* 2012), and, thus, improved the methane decomposition **(**R11**)** and the gasification of carbon deposition.

$$CH_3COCH_3 + 5H_2O \rightarrow 8H_2 + 3CO_2,\ \Delta H^0_{298K} = 246.1\ kJ/mol \quad (R8)$$

$$CH_4 + 2H_2O \rightarrow 4H_2 + CO_2,\ \Delta H^0_{298K} = 165.1\ kJ/mol \quad (R9)$$

$$CH_4 + H_2O \rightarrow 3H_2 + CO,\ \Delta H^0_{298K} = 206.1\ kJ/mol \quad (R10)$$

$$CH_4 \rightarrow C + 2H_2,\ \Delta H^0_{298K} = 74.8\ kJ/mol \quad (R11)$$

$$Coke + O^{2-} \rightarrow CO \rightarrow CO_2 \quad (R12)$$

The effects of S/C on HOAc conversion and gaseous product distributions

The influence of the S/C molar ratios ranging from 1 to 9 on the SRA was investigated at atmospheric and at 600 °C. Table 6 shows the X_{HOAc}, Y_{H2}, as well as the gaseous products concentrations as a function of S/C. At S/C = 1, the X_{HOAc} and Y_{H2} were rather low, and furthermore, there were significant amounts of CO and CH_4. Apparently, higher S/C molar ratios increased the X_{HOAc}, Y_{H2}, as well as the distribution of H_2, while they decreased the CO and CH_4 concentrations. The concentration of CO_2 increased slightly with the S/C. Esteban-Díez *et al.* (2016) and Noor *et al.* (2014) had demonstrated that low S/C molar ratios reduced the methane SR (R9, R10) and WGSR (R2), while they enhanced methanation (R6, R7) simultaneously. Consequently the CH_4 concentration increased as the S/C molar ratio decreased. Therefore, the CH_4 content was a key factor for determining the H_2 selectivity during the SRA process. Hu and Lu (2009) and co-workers pointed out that the high partial pressure of steam at high S/C could promote the steam adsorption on the active sites of catalysts, and consequently inhibited the feedstock degradation and prevented caking. In addition, the high steam pressure was also beneficial for WGSR to reduce the CO content, leading to higher H_2 concentration. Kechagiopoulos *et al.* (2006) had indicated that an excess steam (beyond the stoichiometric limit) was favorable for the suppression of carbon deposition during SR of bio-oil because it promoted the partial gasification of carbon formed, consequently enhancing the conversion of HOAc and intermediates. The results of the present work showed that the catalyst activity in SRA was high with the S/C molar ratio changing from 6 to 9, as in these conditions the Y_{H2} and H_2 content showed high values together with low CH_4 and CO contents.

Table 6. Influence of S/C on HOAc Conversion and Gaseous Products Distributions *

S/C	X_{HOAc} (%)	Y_{H2} (%)	Product concentration (%)			
			H_2	CH_4	CO	CO_2
1	75.2	70.2	51.9	12.2	13.1	22.8
3	90.7	85.6	62.8	4.7	9.3	23.1
6	97.3	87.0	67.7	2.2	4.7	25.4
9	100	90.3	71.3	0.9	1.1	26.7

* -*T*= 600 °C; GHSV = 14427 h^{-1}; atmospheric pressure; time on steam for 4 h

Characterizations of Spent Catalysts

In order to investigate the carbon deposition resistance and sintering extent of these catalysts under harsh operating conditions, the catalysts were tested at low S/C molar ratio (S/C = 1) and 600 °C, GHSV = 14427 h^{-1} for 4 h steam reforming. After reaction, these

spent catalysts were analyzed by XRD, SEM, as well as TG-DSC.

Figure 7 shows the XRD diffraction patterns of all spent catalysts. The diffraction peaks at approximately 2θ = 27° in samples PG and NF/PG belong to the carbon with graphitic structure on these catalysts (Koo *et al.* 2008; Therdthianwong *et al.* 2008). The peaks disappeared after the addition of CeO_2, which was ascribed to the interaction between CeO_2 and PG, promoting the migration of oxygen ions from the interior of CeO_2 to its surface, leading to the gasification of carbon deposition. In addition, the peaks related to the PG and CeO_2 in the XRD patterns were consistent with those found in the XRD patterns before reaction (Fig. 5b). This was explained by the CeO_2 restraining the sintering of active metals during SRA. Furthermore, the diffraction peak located at 2θ = 44.01° was attributed to the Ni-Fe alloy (111) plane and was consistent with the XRD patterns before the reaction (Fig. 5b). Based on the (111) plane of the formed Ni-Fe alloy, the estimated crystallite sizes are shown in Table 5. It was observed that crystallite sizes of formed Ni-Fe alloy were 15.4 nm and 26.3 nm in reduced and spent NF/PG samples, respectively, while they were 8.9 nm and 10.0 nm in reduced and spent NF/$C_{0.4}PG_{0.6}$ samples, respectively. The Ni-Fe alloy in NF/PG underwent significant sintering during SRA, while the Ni-Fe alloy sintering was suppressed by CeO_2 addition NF/$C_{0.4}PG_{0.6}$. It was worth noting that the peaks at 2θ = 51.4° (Fig. 7) presented in all spent catalysts and they were attributed to the characteristic peak of Ni-Fe alloy at (200) lattice plane (Xie *et al.* 2017), while they were unobserved in the after reduced catalysts in Fig. 5b.

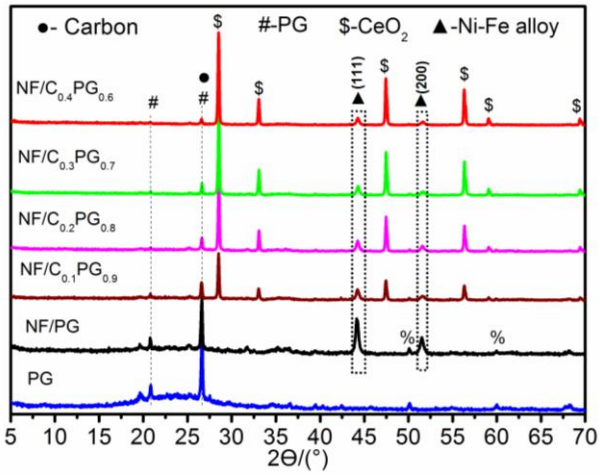

Fig. 7. XRD diffraction patterns of all catalysts after reaction for 4 h at 600 ℃ with S/C = 3 and GHSV = 14427 h^{-1}

Theofanidis and colleagues (2015) designed the carbon-resistant dry reforming Fe-Ni catalyst. After the *in-situ* XRD analysis for reduced sample, they found the Ni-Fe alloy at 2θ = 44° and 51.4°, which was attributed to the (111) and (200) lattice planes, respectively. Kang *et al.* (2016) had also demonstrated the (111) and (200) lattice planes of Ni-Fe alloy emerged in bimetallic Ni-Fe/Al_2O_3 catalysts after the H_2 pre-treatment, which were applied into propane steam reforming for hydrogen production. Therefore, there was no apparent Ni-Fe alloy peak at (200) lattice plane in the present work (Fig. 5b), because Ni-Fe species were highly dispersed on the PG surface and there was strong interaction with the PG. This was mainly due to the high surface area of PG which enhanced the dispersion of active metal, and then, resulted in the Ni-Fe oxides which were difficult to completely reduce. Additionally, the CeO_2 addition also enhanced the

interaction between nickel-iron species and carrier, as demonstrated by H_2-TPR (Fig. 4b), leading to no obvious diffraction peak of Ni-Fe alloy of (200) plane in reduced catalysts.

For the purpose of investigating and comparing the morphology of spent catalysts, the SEM images of fresh and spent catalysts are presented in Fig. 8. Comparison of Figs. 8a and 8c shows that there was a large area of caking and metallic sintering on the surface of the NF/PG sample. The metallic sintering had also been indicated by XRD analysis, and the results are presented in Fig. 5, Fig. 7, as well as Table 5. Consequently the active sites and the filamentous basic structure of PG were packaged by some amount of amorphous carbon, but the filamentous fundamental structure of NF/$C_{0.4}PG_{0.6}$ was clearly shown in Fig. 8d. Thus, the formation of carbon deposition and the caking of catalysts were inhibited by adding CeO_2 (Chiou *et al.* 2014; Vicente *et al.* 2014) because it was well known that CeO_2 has unique redox properties and high oxygen vacancy and mobility, which can promote the gasification of carbonaceous species deposited on a catalyst (Perrichon *et al.* 1994; Zhang *et al.* 2014; Li *et al.* 2015). Figures 8c and 8d also showed that some spherical particles were attached on the surface of catalysts after reaction, wherein the particles attached on the surface of NF/$C_{0.4}PG_{0.6}$ catalyst were in a more uniform distribution than those attached on NF/PG. These particles were attributed to the aggregation of Ni-Fe alloy particles. This result was consistent with previous studies (Tian *et al.* 2013) and was confirmed by the XRD diffraction patterns in Fig. 7.

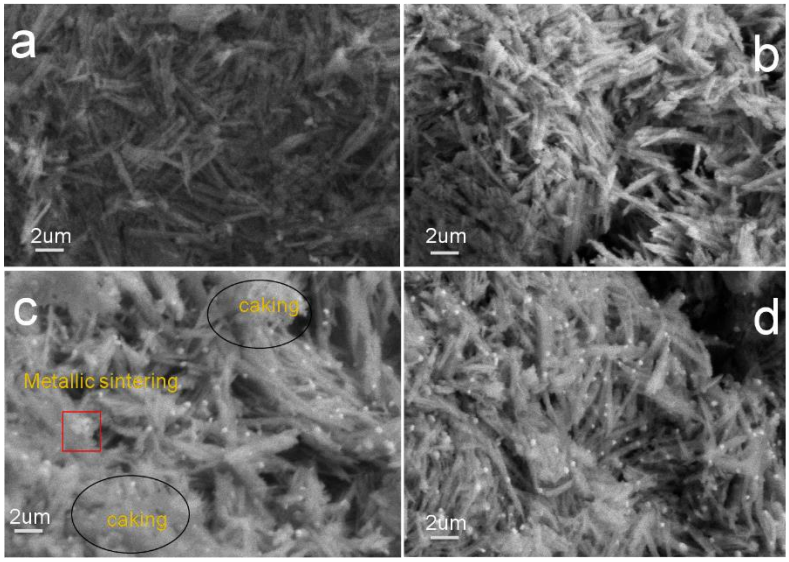

Fig. 8. SEM images of catalysts: (a) fresh NF/PG; (b) fresh NF/$C_{0.4}PG_{0.6}$; (c) spent NF/PG; and (d) spent NF/$C_{0.4}PG_{0.6}$

Metallic nickel is known to be an active catalyst component for SR of hydrocarbons and oxygenates to hydrogen or synthesis gas. Moreover, alloying of Ni with other metals can enhance the catalytic activity and stability, and the iron is a suitable modifier. In addition, the smaller and more uniform Ni-Fe alloy nanoparticles are needed at even high temperature during SR process (Koike *et al.* 2015). Consequently, the catalytic activity sequence: NF/$C_{0.4}PG_{0.6}$ > NF/$C_{0.3}PG_{0.7}$ > NF/$C_{0.2}PG_{0.8}$> NF/$C_{0.1}PG_{0.9}$ > NF/PG (Fig. 6a) during 4 h on steam was attributed to the Ni-Fe alloy crystallite size sequence: NF/$C_{0.4}PG_{0.6}$ < NF/$C_{0.3}PG_{0.7}$ < NF/$C_{0.2}PG_{0.8}$ < NF/$C_{0.1}PG_{0.9}$ < NF/PG (Table 5). Moreover, the activity of every catalyst after 60 min on steam was higher than that in 0 ~ 60 min, as shown in Fig.

6a. This was due to the formation of Ni-Fe alloy with (200) plane (Fig. 7), that increased the active sites of the catalyst. The Ni-Fe alloy (200) came from those unreduced nickel-iron oxides during the active process by reducing gas (as mentioned above) and were further reduced by H_2 in gaseous product.

From the results of XRD and SEM, there was some amount of coke deposited on the surface of spent catalysts. According to Perez-Lopez *et al.* (2006) and Luo *et al.* (2016), the combustion of carbon deposition started at a temperature above 400 °C. So the spent catalysts were analyzed by TGA analysis, in which they were heated in air from room temperature to 900 °C with a ramp of 10 °C/min, to determine the quantity and structure of coke deposited on the catalysts (Nogueira *et al.* 2014). The TG-DSC profiles and the carbon deposition rate are presented in Fig. 9. From the inset map in Fig. 9, the blank test over PG experienced a severe carbon deposited rate of 90.5 mg/($g_{cat.}$·h), while the carbon deposition rate on NF/PG and NF/$_{0.4}$PG$_{0.6}$ were 12.5 mg/($g_{cat.}$·h) and 9.6 mg/($g_{cat.}$·h) respectively. The lower carbon deposition rate for used NF/$_{0.4}$PG$_{0.6}$ was mainly because the coke deposited on the catalyst surface was gasified by the surface oxygen of catalyst, which came from the interior of CeO_2. Since CeO_2 was a superior oxygen carrier and increased the catalyst surface oxygen (as proven by H_2-TPR in Fig. 4). The found carbon deposition rates of NF/PG and NF/$_{0.4}$PG$_{0.6}$ were better than that reported by our previous research (Wang *et al.* 2016), in which 25.9 mg/($g_{cat.}$·h) coke rate was formed on IM-Ni/ATC at 650 °C. Moreover, the carbon deposition amount (3.8%) of NF/$_{0.4}$PG$_{0.6}$ catalyst was lower than the coke amount (9.6%) of spent Ni-Co/La_2O_3 catalyst was researched by Nabgan *et al.* (2016) during the process of SRA. As far as anyone knows, TG-DSC analysis is a complementary technique for estimating the structural order of carbon deposits, because the more ordered carbon structure needs the higher temperature for gasification (Chen *et al.* 2010; Nogueria *et al.* 2014). Fig. 9 shows the DSC profiles of spent catalysts, where it can be seen that carbon deposition oxidation for PG started from 100 °C to 750 °C and the peaks appeared at about 598 °C and 707 °C. According to Nogueria *et al.* (2014), the peak at 220 to 350 °C was assigned to the thermal desorption of absorbed species (H_2O and CO_2) on spent sample and the oxidation of carbonaceous species with low ordered structure like an amorphous type, and the peak at above 500 °C was attributed to the removal of the graphitic or filamentous carbon. Therefore, the exothermic peaks of spent catalysts in this study (Fig. 9) belong to the graphitic or filamentous carbon. However, there were no peaks assigned to the oxidation of amorphous at low temperature. This is because the spent samples had been pre-treated in air by heating to 300 °C to exclude the absorbed species (H_2O and CO_2) affecting the carbon deposition rate. Ultimately, the CeO_2 added into NF/PG not only decreased the carbon deposition rate from 12.5 mg/($g_{cat.}$·h) for NF/PG to 9.6 mg/($g_{cat.}$·h) for NF/$_{0.4}$PG$_{0.6}$, but also partially removed the the graphitic or filamentous structural carbon (also be demonstrated by XRD). Curiously, the exothermic peak of NF/$_{0.4}$PG$_{0.6}$ at 488 °C, which was higher than the oxidation temperature of amorphous type carbon (300 °C) and lower than that of graphitic or filamentous carbon (500 °C). It can be attributed to the carbide with the moderate ordered structure. In other word, this structural carbon was higher ordered carbon compared with amorphous type carbon and a little lower than that of graphitic or filamentous carbon (An *et al.* 2011). Additionally, it had no influence on the activity and stability of catalyst.

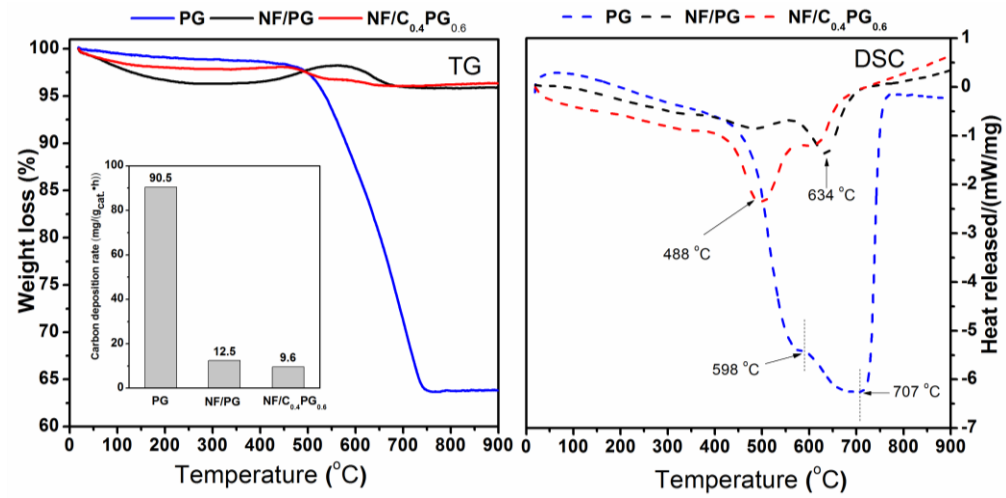

Fig. 9. TGA and DSC profiles of the spent PG, NF/PG, as well as NF/$C_{0.4}PG_{0.6}$.

Stability Tests of NF/PG and NF/$C_{0.4}PG_{0.6}$

Developing highly stable catalysts is one of the major factors in SR reactions. It was found that NF/$C_{0.4}PG_{0.6}$ showed the best performance at 600 °C, S/C of 3, and GHSV = 14427 h^{-1} for 20 h. Moreover, the NF/PG was selected as a counterpart to provide better insight into the catalytic behaviors of NF/$C_{0.4}PG_{0.6}$. Results are shown in Fig. 10. The NF/$C_{0.4}PG_{0.6}$ presented superior stability during the entire time on steam. The H_2 yield and conversion was maintained at about 85% and 95% for 20 h on steam, as shown in Fig. 10b. Conversely, the NF/PG catalyst deactivated significantly after 10 h on steam. The X_{HOAc} and Y_{H2} decreased from about 80% and 55% at the initial test to about 55% and 18 % at the end of the test, respectively (Fig. 10a).

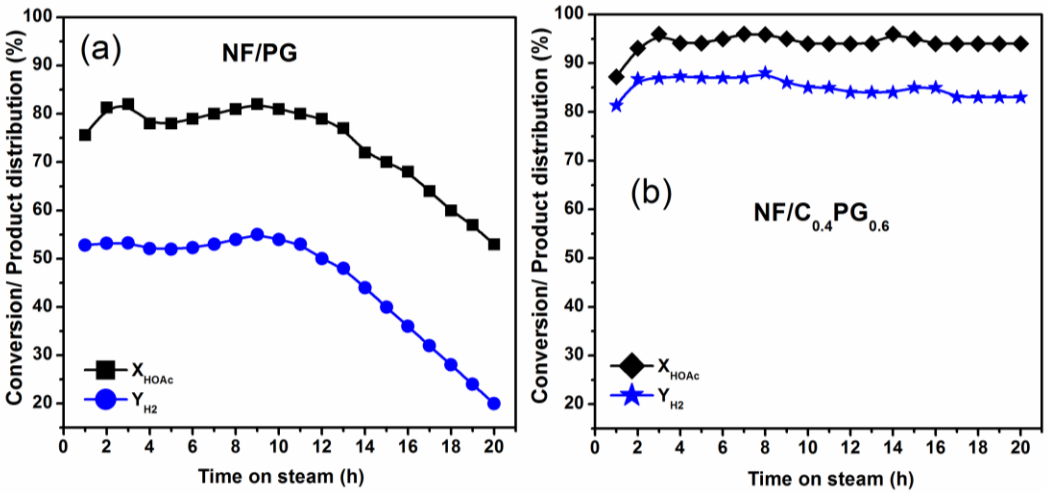

Fig. 10. Stability tests of NF/PG & NF/$C_{0.4}PG_{0.6}$ catalysts: T = 600 °C; S/C = 3; GHSV = 14427 h^{-1}.

DISCUSSION

The catalysts employed by SR technology are invariably subject to serious deactivation mechanisms including coking, sintering of the active phase, and oxidation of

the metallic phase, resulting in the decrease of the active sites on the surface of catalyst and lowering of the catalytic performance to convert carbonaceous compound to C_1 product and hydrogen (Hu and Lu 2010). From the results of XRD and TG-DSC characterizations for reduced and spent catalysts, the CeO_2 not only decreased the crystallite size of Ni-Fe alloy, but also suppressed the carbon deposition rate of catalyst. In addition, the H_2-TPR results further showed the interaction between active phase (Ni-Fe alloy) and CPG support increased by the addition of CeO_2. Consequently, NF/$C_{0.4}PG_{0.6}$ catalyst showed outstanding catalytic activity and stability compared with NF/PG catalyst. In this study, the highest values of X_{HOAc} (95%) and Y_{H2} (85%) were obtained over NF/$C_{0.4}PG_{0.6}$ at 600 °C, S/C of 3, and GHSV = 14427 h^{-1}. Mohanty *et al.* (2012) designed the Cu-Zn/Ca-Al catalyst for SRA and achieved 81% of X_{HOAc} and 80% of Y_{H2} at 800 °C, whereas the results were lower than those found in this study. In addition, the 100% of X_{HOAc} and 73% of Y_{H2} were realized by Bossola and co-workers (2016) on Ru supported on Mg-Al oxides at 700 °C, while the H_2 yield was a little lower than that in this paper. However, the carbon deposition rate in their report (1.9 to 4.9 mg/($g_{cat.}$·h)) was smaller compared with the corresponding result on NF/$C_{0.4}PG_{0.6}$ catalyst (9.6 mg/($g_{cat.}$·h)), because noble metal was always higher than transition metal in terms of anti-carbon deposition. Among the series of Ni/γ-Al_2O_3 with different Ni loading prepared by An *et al.* (2011), 12 wt% Ni/γ-Al_2O_3 showed the best catalytic performance and obtained the highest X_{HOAc} (49%) and Y_{H2} (29%) at 600 °C. In the Ni-Fe bimetallic catalysts, the 10Ni-Fe/ZDA catalyst achieved 100% of X_{HOAc} and 89.6% of Y_{H2} at 700 °C respectively, which was reported by Wang *et al.* (2015) in SRA, whereas they were all slightly decreased after 11 h on steam. Obviously, NF/$C_{0.4}PG_{0.6}$ catalyst had superior catalytic performance among the previous designed steam reforming catalysts and potential value for the industrialization of HOAc steam reforming for hydrogen production.

CONCLUSIONS

1. The results from H_2 temperature programmed reduction (H_2-TPR) and X-ray diffraction (XRD) analyses showed that the addition of CeO_2 increased the hydrogen consumption of catalysts and the interaction force between active component (Ni-Fe alloy) and carrier. Moreover, the Ni-Fe alloys were successfully synthesized in the Ni-Fe/CPG catalysts and their crystallite sizes were decreased by adding CeO_2.
2. The catalyst Ni-Fe/$C_{0.4}PG_{0.6}$ achieved the highest HOAc conversion (95%), highest H_2 yield (87%), and highest H_2 concentration (63%) in gaseous products and enjoyed the most excellent catalytic stability compared with other catalysts in the SRA reaction.
3. The addition of CeO_2 enhanced the stability and activity of Ni-Fe/PG catalysts and decreased the coke deposition rate on the catalyst surface.

ACKNOWLEDGEMENTS

The authors thank the National Natural Science Foundation of China (21376007) and National Science and Technology Support Project of China (2014BAD02B03) for the financial support.

REFERENCES CITED

An, L., Dong, C. Q., Yang, Y. P., Zhang, J. J., and He, L. (2011). "The influence of Ni loading on coke formation in steam reforming of acetic acid," *Renewable Energy* 36(3), 930-935. DOI: 10.1016/j.renene.2010.08.029

Abelló, S, Bolshak, E., and Montané, D. (2013). "Ni-Fe catalysts derived from hydrotalcite-like precursors for hydrogen production by ethanol steam reforming," *Applied Catalysis A General* 450(2), 261-274. DOI: 10.1016/j.apcata.2012.10.035

Basagiannis, A. C., and Verykios, X. E. (2006). "Reforming reactions of acetic acid on nickel catalysts over a wide temperature range," *Applied Catalysis A: General* 308(10), 182-193. DOI: 10.1016/j.apcata.2006.04.024

Basagiannis, A. C., and Verykios, X. E. (2008). "Influence of the carrier on steam reforming of acetic acid over Ru-based catalysts," *Applied Catalysis B: Environmental* 82(1), 77-88. DOI: 10.1016/j.apcatb.2008.01.014

Basagiannis, A. C., and Verykios, X. E. (2007). "Catalytic steam reforming of acetic acid for hydrogen production," *International Journal of Hydrogen Energy* 32(15), 3343-3355. DOI: 10.1016/j.ijhydene.2007.04.039

Bossola, F., Evangelisti, C., Allieta, M., Psaro, R., Recchia, S., and Santo, V. D. (2016). "Well-formed, size-controlled ruthenium nanoparticles active and stable for acetic acid steam reforming," *Applied Catalysis B: Environmental* 181, 599-611. DOI: 10.1016/j.apcatb.2015.08.024

Bolshak, E., Abelló, S., and Montané, D. (2013). "Ethanol steam reforming over Ni-Fe-based hydrotalcites: Effect of iron content and reaction temperature," *International Journal of Hydrogen Energy* 38(14), 5594-5604. DOI: 10.1016/j.ijhydene.2013.02.077

Bulushev, D. A., and Ross, J. R. H. (2011). "Catalysis for conversion of biomass to fuels via pyrolysis and gasification: A review," *Catalysis Today* 171(1), 1-13. DOI: 10.1016/j.cattod.2011.02.005

Blake, P. G., and Jackson, G. E. (1969). "High- and low-temperature mechanisms in the thermal decomposition of acetic acid," *Journal of the Chemical Society B Physical Organic* 1969, 94-96. DOI: 08/03/2017 02:03:12.

Cao, J. L., Shao, G. S., Wang, Y., Liu, Y. P., and Yuan, Z. Y. (2008). "CuO catalysts supported on attapulgite clay for low-temperature CO oxidation," *Catalysis Communications* 9(15), 2555-2559. DOI: 10.1016/j.catcom.2008.07.016

Chattanathan, S. A., Adhikari, S., and Abdoulmoumine, N. (2012). "A review on current status of hydrogen production from bio-oil," *Renewable & Sustainable Energy Reviews* 16(5), 2366-2372. DOI: 10.1016/j.rser.2012.01.051

Chen, J., Yang, X., and Li, Y. D. (2010). "Investigation on the structure and the oxidation activity of the solid carbon produced from catalytic decomposition of methane," *Fuel* 89(5), 943-948. DOI: 10.1016/j.fuel.2009.08.017

Chiou, J. Y. Z., Lai, C. L., Yu, S. W., Huang, H. H., Chuang, C. L., and Wang, C. B. (2014). "Effect of Co, Fe and Rh addition on coke deposition over Ni/Ce0.5Zr0.5O2 catalysts for steam reforming of ethanol," *International Journal of Hydrogen Energy* 39(35), 20689-20699. DOI: 10.1016/j.ijhydene.2014.07.141

Esteban-Díez, G., Gil, M. V., Pevida, C., Chen, D., and Rubiera, F. (2016). "Effect of operating conditions on the sorption enhanced steam reforming of blends of acetic acid and acetone as bio-oil model compounds," *Applied Energy* 2016 177, 579-590. DOI: 10.1016/j.apenergy.2016.05.149

Guo, H. J., Zhang, H. R., Peng, F., Yang, H. J., Xiong, L., Huang, C., Wang, C., Chen, X. D., and Ma, L. L. (2015). "Mixed alcohols synthesis from syngas over activated palygorskite supported Cu-Fe-Co based catalysts," *Applied Clay Science* 111, 83-89. DOI: 10.1016/j.clay.2015.03.009

Hu, X., and Lu, G. X. (2010). "Comparative study of alumina-supported transition metal catalysts for hydrogen generation by steam reforming of acetic acid," *Applied Catalysis B: Environmental* 99(1), 289-297. DOI: 10.1016/j.apcatb.2010.06.035

Hu, X., and Lu, G. (2009). "Investigation of the steam reforming of a series of model compounds derived from bio-oil for hydrogen production," *Applied Catalysis B Environmental* 88(3), 376-385. DOI: 10.1016/j.apcatb.2008.10.021

Iulianelli, A., Liguori, S., Vita, A., Italiano, C., Fabiano, C., Huang, Y., and Basile, A. (2016). "Hydrogen produced in Pd-composite membrane reactor via bioethanol reforming over Ni/CeO_2 catalyst," *Catalysis Today* 259(S2), 368-375. DOI: 10.1016/j.cattod.2015.04.046

Kathe, V. D., Empfield, A., Na, J., Blair, E., and Fan, L. (2016). "Hydrogen production from natural gas using an iron-based chemical looping technology: Thermodynamic simulations and process system analysis," *Applied Energy* 165, 183-201. DOI: 10.1016/j.apenergy.2015.11.047

Kang, K., Azargohar, R., Dalai, A. K., and Wang, H. (2016). "Hydrogen production from lignin, cellulose and waste biomass via supercritical water gasification: Catalyst activity and process optimization study," *Energy Conversion & Management* 117, 528-537. DOI: 10.1016/j.enconman.2016.03.008

Kan, T., Strezov, V., and Evans T. J. (2016). "Lignocellulosic biomass pyrolysis: A review of product properties and effects of pyrolysis parameters," *Renewable and Sustainable Energy Reviews* 57(28), 1126-1140. DOI: 10.1016/j.rser.2015.12.185

Kechagiopoulos, P. N., Voutetakis, S. S., Lemonidou, A. A., and Vasalos, I. A. (2006). "Hydrogen production via steam reforming of the aqueous phase of bio-oil in a fixed bed reactor," *Energy & Fuels* 20(5), 2155-2163. DOI: 10.1021/ef060083q

Koike, M., Li, D. L., Watanabe, H., Nakagawa, Y., and Tomishige, K. (2015). "Comparative study on steam reforming of model aromatic compounds of biomass tar over Ni and Ni-Fe alloy nanoparticles," *Applied Catalysis A: General* 506, 151-162. DOI: 10.1016/j.apcata.2015.09.007

Koo, K. Y., Roh, H. S., Seo,Y. T., Seo, D. J., Yoon, W. L., and Park, S. B. (2008). "Coke study on MgO-promoted Ni/Al_2O_3 catalyst in combined H_2O and CO_2, reforming of methane for gas to liquid (GTL) process," *Applied Catalysis A: General* 340(2), 183-190. DOI: 10.1016/j.apcata.2008.02.009

Li, Z. K., Hu, X., Zhang, L. J., Liu, S. M., and Lu, G. X. (2012). "Steam reforming of acetic acid over Ni/ZrO_2 catalysts: Effects of nickel loading and particle size on product distribution and coke formation," *Applied Catalysis A: General* s417-418(1), 281-298. DOI: 10.1016/j.apcata.2012.01.002

Laosiripojana, N., Sutthisripok, W., Assabumrungrat, S., and Assabumrungrat, S. (2014). "Development of Ni-Fe bimetallic based catalysts for biomass tar cracking/reforming: Effects of catalyst support and co-fed reactants on tar conversion characteristics," *Fuel Processing Technology* 127(11), 26-32. DOI: 10.1016/j.fuproc.2014.06.015

Li, X. Z., Hu, Z. L., Zhao, H. B., and Lu, X. W. (2013). "$Ce_{1-x}Sm_xO_{2-\delta}$-attapulgite nanocomposites: Synthesis *via* simple microwave approach and investigation of its catalytic activity," *Journal of Rare Earths* 31(12), 1157-1162. DOI: 10.1016/S1002-0721(12)60420-7

Li, Y., Wang, X. X., and Song, C. S. (2015). "Spectroscopic characterization and catalytic activity of Rh supported on CeO_2-modified Al_2O_3 for low-temperature steam reforming of propane," *Catalysis Today* 263, 22-34. DOI: 10.1016/j.cattod.2015.08.063

Luo, X., Hong, Y., Wang, F. C., Hao, S. Q., Pang, C. H., Lester, E., and Wu, T. (2016). "Development of nano Ni_xMg_yO solid solutions with outstanding anti-carbon deposition capability for the steam reforming of methanol," *Applied Catalysis B Environmental* 194, 84-97. DOI: 10.1016/j.apcatb.2016.04.031

Lytkina, A. A., Zhilyaeva, N. A., Ermilova, M. M., Orekhova, N. V., and Yaroslavtsev, A. B. (2015). "Influence of the support structure and composition of Ni-Cu-based catalysts on hydrogen production by methanol steam reforming," *International Journal of Hydrogen Energy* 40(31), 9677-9684. DOI: 10.1016/j.ijhydene.2015.05.094

Mei, D. H., Dagle, V. L., Xing, R., Albrecht, K. O., and Dagle, R. A. (2016). "Steam reforming of ethylene glycol over $MgAl_2O_4$ supported Rh, Ni, and Co catalysts," *ACS Catalysis* 6(1), 315-325.DOI: 10.1021/acscatal.5b01666

Mohanty, P., Patel, M., and Pant, K. K. (2012). "Hydrogen production from steam reforming of acetic acid over Cu-Zn supported calcium aluminate," *Bioresource Technology* 123(3), 558-565. DOI: 10.1016/j.biortech.2012.07.019

Ma, Z., Zhang, S. P., Xie, D. Y., and Yan, Y. J. (2014). "A novel integrated process for hydrogen production from biomass," *International Journal of Hydrogen Energy* 39(3), 1274-1279.DOI: 10.1016/j.ijhydene.2013.10.146

Marquevich, M., Czernik, S., Chornet, E., and Montane´, D. (1999). "Hydrogen from biomass: Steam reforming of model compounds of fast-pyrolysis oil," *Energy & Fuels* 13(6), 1160-1166. DOI: 10.1021/ef990034w

Nogueira, F. G. E., Assaf, P. G. M., Carvalho, H. W. P., and Assaf, E. M. (2014). "Catalytic steam reforming of acetic acid as a model compound of bio-oil," *Applied Catalysis B: Environmental* 166-161(7), 188-199. DOI: 10.1016/j.apcatb.2014.05.024

Noor, T, Gil, M. V., and Chen, D. (2014). "Production of fuel-cell grade hydrogen by sorption enhanced water gas shift reaction using Pd/Ni-Co catalysts," *Applied Catalysis B Environmental* 150-151(18), 585-595. DOI: 10.1016/j.apcatb.2014.01.002

Nabgan, W., Abdullah, T. A. T., Mat, R., Nabgan, B., Jalil, A. A., Firmansyah, L., and Triwahyono, S. (2016). "Production of hydrogen via steam reforming of acetic acid over Ni and Co supported on La_2O_3 catalyst," *International Journal of Hydrogen Energy* 4(176), 1-11. DOI: 10.1016/j.ijhydene.2016.04.176

Olaleye, A. K., Adedayo, K. J., Wu, C. F., Nahil, M. A., Wang, M. H. and Williams, P. T. (2014). "Experimental study, dynamic modelling, validation and analysis of hydrogen production from biomass pyrolysis/gasification of biomass in a two-stage fixed bed reaction system," *Fuel* 137(6), 364-374. DOI: 10.1016/j.fuel.2014.07.076

Osorio-Vargas, P., Flores-González, N. A., Navarro, R. M., Fierro, J. L. G., Campos, C. H., and Reyes, P. (2016). "Improved stability of Ni/Al_2O_3 catalysts by effect of promoters (La_2O_3, CeO_2) for ethanol steam-reforming reaction," *Catalysis Today* 259, 27-38. DOI: 10.1016/j.cattod.2015.04.037

Pant, K. K., Mohanty, P., Agarwal, S., and Dalai, A. K. (2013). "Steam reforming of acetic acid for hydrogen production over bifunctional Ni-Co catalysts," *Catalysis Today* 207(207), 36-43. DOI: 10.1016/j.cattod.2012.06.021

Pandey, D., and Deo, G. (2016). "Effect of support on the catalytic activity of supported

Ni-Fe catalysts for the CO_2 methanation reaction," *Journal of Industrial and Engineering Chemistry* 33(25), 99-107. DOI: 10.1016/j.jiec.2015.09.019

Perrichon, V., Laachir, A., Bergeret, G., Frety, R., and Tournayan, L. (1994). "Reduction of cerias with different textures by hydrogen and their reoxidation by oxygen," *Journal of the Chemical Society Faraday Transactions* 90(5), 773-781. DOI: 10.1039/FT9949000773

Perez-Lopez, O. W., Senger, A., Marcilio, N. R., and Lansarin, M. A. (2006). "Effect of composition and thermal pretreatment on properties of Ni-Mg-Al catalysts for CO_2 reforming of methane," *Applied Catalysis A General* 303(2), 234-244. DOI: 10.1016/j.apcata.2006.02.024

Pimenidou, P., Rickett, G., Dupont, V., and Twigg, M. V. (2010). "Chemical looping reforming of waste cooking oil in packed bed reactor," *Bioresource Technology* 101(16), 6389-6397. DOI: 10.1016/j.biortech.2010.03.053

Rapagná, S., Provendier, H., Petit, C., Kiennemann, A., and Foscolo, P. U. (2002). "Development of catalysts suitable for hydrogen or syn-gas production from biomass gasification," *Biomass and Bioenergy* 22(5), 377-388. DOI: 10.1016/S0961-9534(02)00011-9

Remiro, A., Valle, B., Aguayo, A. T., Bilbao, J., and Gayubo, A. G. (2013). "Operating conditions for attenuating Ni/La_2O_3-αAl_2O_3, catalyst deactivation in the steam reforming of bio-oil aqueous fraction," *Fuel Processing Technology* 115, 222-231. DOI: 10.1016/j.fuproc.2013.06.003

Ramesh, S., Yang, E. H., Jung, J. S., and Moon, D. J. (2015). "Copper decorated perovskite an efficient catalyst for low temperature hydrogen production by steam reforming of glycerol," *International Journal of Hydrogen Energy* 40(35), 11428-11435. DOI: 10.1016/j.ijhydene.2015.02.013

Shen, D. K., Jin, W., Hu, J., Xiao, R., and Luo, K. H. (2015). "An overview on fast pyrolysis of the main constituents in lignocellulosic biomass to valued-added chemicals: Structures, pathways and interactions," *Renewable and Sustainable Energy Reviews* 51(6), 761-774. DOI: 10.1016/j.rser.2015.06.054

Świerczyński, D., Libs, S., Courson, C. A., and Kiennemann, A. (2007). "Steam reforming of tar from a biomass gasification process over Ni/olivine catalyst using toluene as a model compound," *Applied Catalysis B: Environmental* 74(3-4), 211-222. DOI: 10.1016/j.apcatb.2007.01.017

Theofanidis, S. A., Galvita, V. V., Poelman, H., and Marin, G. B. (2015). "Enhanced carbon-resistant dry reforming Fe-Ni catalyst: Role of Fe," *Acs Catalysis* 2015, 3028-3039. DOI: 10.1021/acscatal.5b00357

Therdthianwong, S., Siangchin, C., and Therdthianwong, A. (2008). "Improvement of coke resistance of Ni/Al_2O_3, catalyst in CH_4/CO_2 reforming by ZrO_2 addition," *Fuel Processing Technology* 89(2), 160-168. DOI: 10.1016/j.fuproc.2007.09.003

Tian, D. Y., Liu, Z. H., Li, D. D., Shi, H. L., Pan, W. X., and Cheng, L. (2013). "Bimetallic Ni–Fe total-methanation catalyst for the production of substitute natural gas under high pressure," *Fuel* 104, 224-229. DOI: 10.1016/j.fuel.2012.08.033

Trane, R., Dahl, S., Skjøth-Rasmussen, M. S., and Jensen, A. D. (2012). "Catalytic steam reforming of bio-oil," *International Journal of Hydrogen Energy* 37(8), 6447-6472. DOI: 10.1016/j.ijhydene.2012.01.023

Vagia, E. C., and Lemonidou, A. A. (2007). "Thermodynamic analysis of hydrogen production via steam reforming of selected components of aqueous bio-oil fraction," *International Journal of Hydrogen Energy* 32(2), 212-223. DOI:

10.1016/j.ijhydene.2006.08.021
Vicente, J., Montero, C., Ereña, J., Azkiti, M. J., Bilbao, J., and Gayubo, A. G. (2014). "Coke deactivation of Ni and Co catalysts in ethanol steam reforming at mild temperatures in a fluidized bed reactor," *International Journal of Hydrogen Energy* 39(24), 12586-12596. DOI: 10.1016/j.ijhydene.2014.06.093
Wang, D., Montané, D., and Chornet, E. (1996). "Catalytic steam reforming of biomass-derived oxygenates: Acetic acid and hydroxyacetaldehyde,' *Applied Catalysis A General* 143(2), 245-270. DOI: 10.1016/0926-860X(96)00093-2
Wang, Q., Wang, S. R., Li, X. B., and Guo, L. (2013). "Hydrogen production via acetic acid steam reforming over HZSM-5 and Pd/HZSM-5 catalysts and subsequent mechanism studies," *BioResources* 8(2), 2897-2909. DOI:(.We cannot find the DOI of this literature.)
Wang, S. R., Li, X. B., Guo, L., and Luo, Z. Y. (2012). "Experimental research on acetic acid steam reforming over Co-Fe catalysts and subsequent density functional theory studies," *International Journal of Hydrogen Energy* 37(37), 11122-11131. DOI: 10.1016/j.ijhydene.2012.05.011
Wang, Y. S., Chen, M. Q., Liang, T., Yang, Z. L., Yang, J., and Liu, S. M. (2016). "Hydrogen generation from catalytic steam reforming of acetic acid by Ni/attapulgite catalysts," *Catalysts* 6(11), 172. DOI: 10.3390/catal6110172
Wang, Y. S., Chen, M.Q., Liu, S. M., Yang, Z. L., Shen, C. P., and Liu, K. (2015). "Hydrogen production via catalytic steam reforming of bio-oil model compounds over NiO-Fe_2O_3-loaded palygouskite," *Journal of Fuel Chemistry and Technology* 43(12), 1470-1475.
Wang, L., Li, D. L., Koike, M., Koso, S., Nakagawa, Y., Xu, Y., and Tomishige, K. (2011). "Catalytic performance and characterization of Ni-Fe catalysts for the steam reforming of tar from biomass pyrolysis to synthesis gas," *Applied Catalysis A: General* 392(1-2), 248-255. DOI: 10.1016/j.apcata.2010.11.013
Wu, C. F., Wang, L. Z., Williams, P. T., Shi, J., and Huang, J. (2011). "Hydrogen production from biomass gasification with Ni/MCM-41 catalysts: Influence of Ni content," *Applied Catalysis B: Environmental* 108(108), 6-13. DOI: 10.1016/j.apcatb.2011.07.023
Wu, C. F., Wang, Z. C., Dupont, V., Huang, J., and Williams, P. T. (2013). "Nickel-catalysed pyrolysis/gasification of biomass components," *Journal of Analytical & Applied Pyrolysis* 99(1), 143-148. DOI: 10.1016/j.jaap.2012.10.010
Xie, C., Wang, Y. Y., Hu, K., Tao, L., Huang, X. B., Huo, J., and Wang, S. Y. (2017). "In situ confined synthesis of molybdenum oxide decorated nickel-iron alloy nanosheets from MoO_4^{2-} intercalated layered double hydroxides for the oxygen evolution reaction," *Journal of Materials Chemistry A* 5(87), 87-91. DOI: 10.1039/c6ta08149e
Yue, Y. Z., Liu, F., Zhao, L., Zhang, L. H., and Liu, Y. (2015). "Loading oxide nano sheet supported Ni-Co alloy nanoparticles on the macroporous walls of monolithic alumina and their catalytic performance for ethanol steam reforming," *International Journal of Hydrogen Energy* 40(22), 7052-7063. DOI: 10.1016/j.ijhydene.2015.04.036
Yao, H. C., and Yao, Y. F. Y. (1984). "Ceria in automotive exhaust catalysts: I. Oxygen storage," *Journal of Catalysis* 86(2), 254-265. DOI: 10.1016/0021-9517(84)90371-3
You, J., Chen, F., Zhao, X. B., and Chen, Z. G. (2010). "Preparation, characterization and catalytic oxidation property of CeO_2/Cu^{2+}-attapulgite (ATP) nanocomposites,"

Journal of Rare Earths 28(S1), 347-352. DOI: 10.1016/S1002-0721(10)60328-6

Zhang, Y., Kajitani, S., Ashizawa, M., and Oki, Y. (2010). "Tar destruction and coke formation during rapid pyrolysis and gasification of biomass in a drop-tube furnace," *Fuel* 89(2), 302-309. DOI: 10.1016/j.fuel.2009.08.045

Zhang, C. X., Li, S. R., Wu, G. W., and Gong, J. L. (2014). "Synthesis of stable Ni-CeO_2 catalysts via ball-milling for ethanol steam reforming," *Catalysis Today* 233(13), 53-60. DOI: 10.1016/j.cattod.2013.08.013

Zhang, M. H., Jiang, D. Y., and Jiang, H. X. (2012). "Enhanced oxygen storage capacity of $Ce_{0.88}Mn_{0.12}O_y$ compared to CeO_2: An experimental and theoretical investigation," *Materials Research Bulletin* 47(12), 4006-4012. DOI: 10.1016/j.materresbull.2012.08.07

Article submitted: November 23, 2016; Peer review completed: January 28, 2017; Revised version received and accepted: March 29, 2017; Published: May 16, 2017.
DOI: 10.15376/biores.12.3.4830-4853